Applied Surface Science 571 (2022) 151282

Contents lists available at ScienceDirect

Applied Surface Science

journal homepage: www.elsevier.com/locate/apsusc

Full Length Article

Investigation of abnormally high growth-per-cycle in atomic layer deposition of Al_2O_3 using trimethylaluminum and water

So-Yeon Ham [1], Zhenyu Jin, Seokhee Shin, Minseo Kim, Mingyu Seo, Yo-Sep Min [*]

Department of Chemical Engineering, Konkuk University, 120, Neungdong-Ro, Gwangjin-Gu, Seoul 05029, Republic of Korea

ARTICLE INFO

Keywords:
Atomic layer deposition (ALD)
Growth-per-cycle (GPC)
Alumina
Trimethylaluminum (TMA) and water
Abnormally high GPC

ABSTRACT

Atomic layer deposition (ALD) has the excellent advantage of precisely controlling the thickness of thin films at the atomic scale owing to the self-limiting chemisorption of precursors, but its low growth-per-cycle (GPC) is a weakness in applications requiring thick films. Under the saturation process conditions for the self-limiting growth behavior in Al_2O_3 ALD using trimethylaluminum (TMA) and H_2O, the GPC values are limited to approximately 1–1.2 Å/cycle in the temperature range of 80–250 °C. However, in the practical use of the Al_2O_3 ALD, abnormally high GPC often occurs, which is generally regarded as the failure to control saturation conditions such as insufficient water purge. Based on comparisons of the normal ALD processes and various modified ALD processes with abnormally high GPC, we report that the unusually high GPC in the Al_2O_3 ALD is not only caused by the residual H_2O but also due to the dimeric nature of TMA. Dimeric aggregate fragments of TMA and dimethylaluminum hydroxide were identified by quadrupole mass spectrometry during TMA exposure and Ar purge steps. This observation supports the dimeric interaction of TMA with the residual H_2O.

1. Introduction

Atomic layer deposition (ALD) is a deposition technique to grow thin films via the chemical adsorption of precursor molecules [1]. ALD has several advantages such as outstanding conformality and precise thickness controllability at atomic scale owing to its self-limiting growth behaviour [1–3]. As the semiconductor industry demands more compact and miniaturized structures, ALD has emerged as an indispensable process for depositing ultrathin and conformal films [4–6]. ALD is often compared to chemical vapor deposition (CVD) in that both techniques chemically deposit thin films from precursor vapors in a vacuum chamber. Since the precursors in CVD are simultaneously supplied to the substrate at high temperatures, various chemical reactions occur in the gas phase and/or at the interface of gas and solid phases including thermal decomposition. However, in ALD, thin film growth is achieved at low temperatures only by chemical adsorption by repeating an ALD cycle. For binary thin films such as Al_2O_3, the ALD cycle generally consists of four sequential steps: the first precursor exposure (e.g., Al precursor), purge, the second precursor exposure (e.g., O precursor), and purge. Since each exposure of the two precursors is separated by the purge step to remove byproducts and residual precursors, the growth of the thin film is attributed to chemical adsorption and is self-limiting against the exposure of precursors.

The thickness increment per cycle under saturation conditions for the self-limiting chemisorption is called growth-per-cycle (GPC). The GPC of ALD is limited by the theoretical maximum of monolayer thickness [7]. For an amorphous Al_2O_3 film with a density of 3.3 g/cm^3, the theoretical monolayer thickness is ~2.95 Å [8]. In general, the growth rate (i.e., GPC) of ALD is much lower than that of CVD. Since the low GPC of ALD is a critical problem in industrial applications for mass production, various attempts have been made to overcome the low GPC by improving the throughput of ALD with a modified chamber design [9]. Gordon et al. reported an intriguing approach for rapid ALD which deposits conformal films of silicon oxide and aluminum oxide nanolaminates with trimethylaluminum (TMA) and tris(*tert*-butoxy)silanol via catalytic insertion of silanol molecules into the Al—O bonds with a GPC value of 12 nm/cycle [10]. However, since GPC is inherently dependent on the surface chemistry of precursor molecules and the adsorption sites, the GPC values are usually determined by the choice of the ALD precursors. As another approach to achieve higher GPC values, exposure of multiple short-pulses, instead of a single pulse of precursor molecules, has been proposed to further utilize the adsorption sites

* Corresponding author.
E-mail address: ysmin@konkuk.ac.kr (Y.-S. Min).
[1] Current affiliation: Materials Science and Engineering Program, University of California San Diego, 9500 Gilman Drive, La Jolla, San Diego, CA 92093, USA.

https://doi.org/10.1016/j.apsusc.2021.151282
Received 24 July 2021; Received in revised form 5 September 2021; Accepted 11 September 2021
Available online 15 September 2021

sterically hindered by the bulkiness of ligands [11–13]. However, the thickness increment per cycle by the exposure of multiple short-pulses cannot exceed the theoretical monolayer thickness of the material (e.g., ~2.95 Å for Al_2O_3) because the number of adsorption sites is limited on the surface.

Al_2O_3 ALD is one of the most extensively studied processes among various ALD chemistries. TMA and water (or a combination of TMA and ozone) are the most used precursors for Al_2O_3 ALD. The generally accepted mechanism consists of two half-reactions upon exposure to TMA and water, respectively.

$$n \text{ ⊩OH} + \text{Al(CH}_3\text{)}_3\text{(g)} \rightarrow \text{(⊩O)}_n\text{Al(CH}_3\text{)}_{3-n} + n\text{CH}_4\text{(g)} \quad (1)$$

$$\text{⊩Al(CH}_3\text{)}_{3-n} + (3-n)\text{H}_2\text{O(g)} \rightarrow \text{⊩Al(OH)}_{3-n} + (3-n)\text{CH}_4\text{(g)} \quad (2)$$

where the symbol ⊩ denotes the surface species and $n = 1$ or 2 in general [14]. In the temperature range of 80–250 °C, the GPC values of the TMA/water process are approximately 1–1.2 Å/cycle under the saturation conditions for self-limiting growth [8,15,16]. However, in practice, users of ALD equipment often experience abnormally high GPC with poor uniformity. This is generally believed to be mainly due to insufficient purge of water, resulting in CVD-like reactions [17]. Recently, Salami et al. reported anomalously high GPC values of Al_2O_3 ALD using TMA and water, which are more than twice the GPC value of ~1.1 Å/cycle obtained under the saturation conditions [18]. The unusually high GPC values were observed when the TMA dose was switched to underdosing conditions as the TMA dose was reduced while the water dose was held constant. Furthermore, the Al_2O_3 films grown under the underdosing condition exhibited excellent thickness uniformity as the films grown under the saturation conditions. They concluded that the underdosing of TMA produces a partially methylated surface, thus water molecules supplied in the subsequent step can be additionally adsorbed on the surface through hydrogen bonding with surface hydroxyl groups, and the molecular adsorption of water provides additional pathways for Al_2O_3 growth.

On the other hand, TMA exists mostly as a dimer (Al_2Me_6) in vapor and liquid phases at room temperature since Al atoms prefer a tetra-coordinated structure rather than a tri-coordinated structure [19–21]. The dimer structure contains two penta-coordinated carbon atoms in the bridged methyl groups (Scheme 1a) [22,23]. Note that there are two kinds of methyl groups in the dimers, bridged and terminal CH_3 groups. The dissociation energy of the dimer is ~20.2 kcal/mol (i.e., 84.5 kJ/mol or 0.88 eV) [19], which is comparable to the heat of adsorption of water on alumina [24]. Since the dimeric TMA dissociates readily at higher temperatures, the average molecular weight of TMA decreases from the molecular weight (144.17 g/mol) of the dimer to that (72.09 g/mol) of the monomer with increasing temperature. For example, the degree of dissociation of the dimer increases with increasing temperature as follows: ~0.075 (100.3 °C), ~0.118 (115.0 °C), and ~0.340 (155.7 °C) [19].

According to several previous reports [25–29], TMA molecules are chemically adsorbed forming dimeric adsorbates at low temperatures (e.g., room temperature) when exposed to various surfaces such as silica, alumina, and silicon. In addition to the chemisorbed layer, TMA also forms a weakly bound multilayer consisting of molecular dimers [25,26,29]. Salaneck and co-workers reported that the TMA adsorbed on Si exists as a dimer whose long molecular axis is approximately perpendicular to the surface [26]. Furthermore, due to the significant amount of dissociation energy of dimers, the multilayered TMA molecules can be removed by prolonged evacuation (~10 min) at room temperature [29]. Gow et al. reported that the TMA dimers adsorbed on Si at low temperature dissociate into monomers upon heating to 300–400 K [27,28]. Moreover, Hackler and co-workers recently identified the dimeric methylalumina surface species at 70 °C during Al_2O_3 ALD on Ag from TMA and water using operando surface-enhanced Raman spectroscopy (Scheme 1b) [30,31].

(a) TMA dimer (Ref. 21) (b) TMA dimer on surface (Ref. 31)

Scheme 1. Dimeric structures of TMA in gas/liquid phases (a) and on surface (b) reported in literatures (Me = CH_3) [21,31].

Given the non-negligible dissociation energy of dimeric interaction, we infer that the dimeric interaction of TMA can occur on the surface and may affect the GPC of Al_2O_3 ALD using TMA and water depending on the process conditions. Here we systematically performed ALD sequences which are modified to split the exposure times of TMA and/or water into equal pulse times while the cumulative exposure time of each precursor is held constant. Split exposures of TMA after sufficient water exposure results in higher GPC with increasing the number of splits. In this work, the abnormally high GPC values are discussed in terms of the dimeric nature of TMA.

2. Experimental

Al_2O_3 films were deposited on boron-doped Si (1 0 0) wafers (6 in., 10.0 ohm·cm, LG Siltron, Inc.) in laminar flow-type ALD equipment with a cold-wall reactor (ATOMIC-CLASSIC, CN1 Co., Ltd.). TMA (99.999%, iChems Co., Ltd.) and deionized water were used as precursors of aluminum and oxygen, respectively. Both precursors were stored in each canister at room temperature and delivered to the reactor by vacuum without carrier gas to avoid confusion in mass spectrometric analysis. Since TMA has a high vapor pressure of ~8.4 torr at room temperature [19], surface saturation for the self-limiting growth can be achieved by delivering TMA without a carrier gas (see Fig. S2). The gas delivery lines were maintained at 100 °C to prevent condensation of the precursors before reaching the reactor. After each precursor exposure, nitrogen gas (99.999%, Daedong Seongdong Oxygen) was flowed at a flow rate of 400 sccm to purge the reactor for removal of residual precursors and byproducts. ALD was performed in a temperature range of 80 to 250 °C, and the process temperature was calibrated with a thermocouple-implanted silicon wafer under an N_2 atmosphere of 1 torr.

In this work, two types of ALD processes were performed for comparison: the normal process and the modified process. Both the normal process and the modified process can be expressed as:

$$[(\text{TMA} - \text{purge})_{x+1} - (\text{water} - \text{purge})_{y+1}]_n$$

where n is the number of ALD cycles, and x and y represent the number of splits for TMA and water, respectively (Fig. S1). Given a cumulative TMA exposure time (t_{TMA}) per cycle, each TMA pulse time (t'_{TMA}) in one cycle is related as $t'_{TMA} = t_{TMA}/(x+1)$. Similarly, $t'_{Water} = t_{Water}/(y+1)$ for water. The normal ALD process corresponds to the case of $x = 0$ and $y = 0$ and can be expressed as $[(\text{TMA} - \text{purge})_1 - (\text{water} - \text{purge})_1]_n$. Thus, $t'_{TMA} = t_{TMA}$ and $t'_{Water} = t_{Water}$ in the normal ALD process. In this work, the normal ALD process was performed with $t_{TMA} = t'_{TMA} = 1.2$ s and $t_{Water} = t'_{Water} = 1.2$ s, and the purge times were 10 s. If the cumulative TMA exposure time ($t_{TMA} = 1.2$ s) is split once ($x = 1$ and $y = 0$) for the modified process, it is expressed as $[(\text{TMA} - \text{purge})_2 - (\text{water} - \text{purge})_1]_n$, where $t'_{TMA} = t_{TMA}/2 = 0.6$ s and $t_{Water} = t'_{Water} = 1.2$ s. Unless otherwise stated for the modified process, the cumulative exposure time per cycle was 1.2 s for both TMA and water, and the purge times were 10 s.

A spectroscopic ellipsometer (SE, MG-1000, Nano-View Co., LTD.) was used to measure the thicknesses of Al_2O_3 films. The spectral range of SE was 1.5–5.0 eV, and the incident angle of the light was fixed at 70°.

The native oxide thickness (~15 Å) was measured before each ALD process and was excluded when measuring the Al_2O_3 film thickness. X-ray photoelectron spectroscopic (XPS) analysis was performed with a Thermo K-alpha XPS system (Thermo Fisher Scientific) using a monochromatic Al Kα X-ray source. During XPS measurements, electrons were sprayed with a flood gun to prevent peak shifting due to the charging effect. For depth profiling by XPS, Al_2O_3 films were sputtered with an argon ion beam (2 keV).

Quadrupole mass spectrometer (QMS, Dymaxion Residual Gas Analyzer, AMETEK) was used to monitor fragments of gaseous species during Al_2O_3 ALD. Samplings of the gaseous species from the ALD reactor to the mass spectrometer were accomplished using a 150 μm orifice, and the delivery line between them was heated to 80 °C to prevent condensation. The ionization energy was 70 eV, and the dwell time was set to 30 ms. For the QMS analysis, the sequence of Al_2O_3 ALD was TMA (40 s)–Ar (400 s)–H_2O (40 s)–Ar (560 s), and the purge gas was replaced with argon because nitrogen gas has a peak overlapping with TMA at $m/z = 28$.

3. Results and discussion

Fig. 1 shows the thickness variation of Al_2O_3 film grown at 80 °C for 100 cycles against the number of splits. As explained in the experimental section, x and y indicate the number of splits for TMA and water, respectively. The thickness of Al_2O_3 grown by the normal ALD (the data at $x = y = 0$ in Fig. 1a and b) is 112 Å (±3.3) which is in good agreement with previous reports [15,16]. However, in Fig. 1a wherein the TMA exposure time ($t_{TMA} = 1.2$ s) was split x times while the water exposure time ($t_{Water} = 1.2$ s) was not split ($y = 0$), thickness grown by the modified ALD tends to increase as the number of splits for TMA (x) increases, depending on how many times the cumulative TMA exposure time ($t_{TMA} = 1.2$ s) is split. For the case of $x = 3$ and $y = 0$, the Al_2O_3 thickness is ~334 Å (±21), which is three times the thickness by the normal process and is thicker than the theoretical monolayer thickness of Al_2O_3 (~2.95 Å). However, the uniformity of films expressed as the standard deviation in a 6-in. wafer is severely poor in the modified process. XPS depth profiles of the films grown at 80 °C by the normal and modified processes (Fig. S3) are in good agreement with the stoichiometric ratio (O/Al = 1.5) of Al_2O_3. The carbon residues (1–3%) are observed in both thin films. Therefore, there is no significant difference in the composition of both thin films despite the three-fold difference in GPC.

In Fig. 1b, both exposure times ($t_{TMA} = t_{Water} = 1.2$ s) of TMA and water were split while maintaining $x = y$. However, increasing the number of splits for water does not result in a further increase in Al_2O_3 thickness comparing to Fig. 1a. This reveals that insufficient water purge is not the main cause of the abnormal GPC since the cumulative water purge time increases from 10 ($y = 0$) to 40 s ($y = 3$) with the number of splits for water.

Fig. 2 compares the splitting effect of TMA exposure time at deposition temperatures of 80, 150, and 250 °C. The thickness increase by the split pulses of TMA was also observed at 150 °C similarly to 80 °C, but not at 250 °C. Because a high temperature of ~200 °C is required to remove water molecules adsorbed on the Al_2O_3 surface [24], the absence of abnormally high GPC at 250 °C raises suspicion of the insufficient water purge. However, this is not the case as explained in Fig. 3. For comparison with Al_2O_3 ALD, we performed ZnO ALD at 150 °C using diethylzinc (DEZ) and water by the modified process in which the DEZ exposure time ($t_{DEZ} = 1.2$ s) was split x times while the water exposure time ($t_{Water} = 1.2$ s) was not split ($y = 0$). Since DEZ undergoes a vigorous exothermic reaction with hydroxyls and water as much as TMA, if residual water molecules were the only cause of the abnormally high GPC, the splitting effect should also appear in ZnO ALD at 150 °C. However, there was no splitting effect in ZnO ALD in Fig. 3. It is worth noting that DEZ, unlike TMA, has a monomeric structure in gas and liquid phases.[32] Thus, it reveals that the abnormally high GPC is related to the dimeric nature of TMA. The detailed discussion regarding the dimeric interaction will be presented in the following paragraph for QMS analysis.

For comparison, we performed Al_2O_3 ALD using two combinations of precursors (TMA/water and TMA/O_3) by modified processes. In Fig. 4, the TMA exposure time ($t_{TMA} = 1.2$ s) was split x times while the exposure time of oxygen precursor ($t_{Water} = 1.2$ s or $t_{Ozone} = 1.2$ s) was not split ($y = 0$). Unlike the TMA/water combination, the modified process using TMA/O_3 does not result in any splitting effect on film thickness. According to previous infrared studies of surface reactions in Al_2O_3 ALD using TMA and ozone [33,34], surface hydroxyls are produced when the TMA-pulsed surface is exposed to ozone, although the surface hydroxyl concentration is lower than that of the TMA/water process. Therefore, it can be inferred that the abnormal thickness increase by the split of TMA exposure time is caused by the cooperative effect of the dimeric nature of TMA and residual water molecules adsorbed on the surface, rather than the effect acting alone by the dimeric interaction or residual water molecules.

As aforementioned in Fig. 1, the key steps for the abnormally high

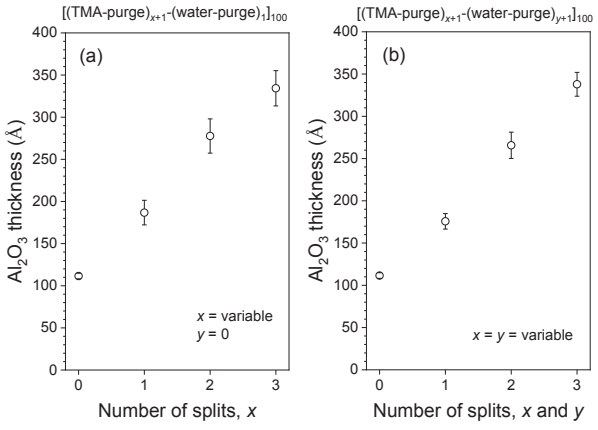

Fig. 1. Al_2O_3 thickness grown for 100 cycles at 80 °C against the number of splits. (a) The TMA exposure time ($t_{TMA} = 1.2$ s) was split x times while the water exposure time ($t_{Water} = 1.2$ s) was not split ($y = 0$). (b) Both exposure times ($t_{TMA} = t_{Water} = 1.2$ s) of TMA and water were split while maintaining $x = y$. The purge times were 10 s for both precursors. The error bar denotes the standard deviation of Al_2O_3 thickness in a 6-in. wafer.

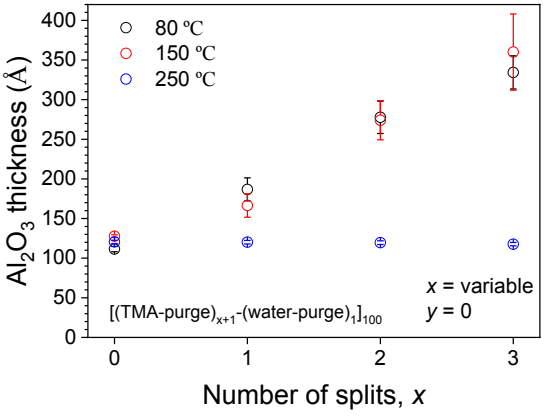

Fig. 2. Al_2O_3 thickness grown for 100 cycles at 80 (black), 150 (red), and 250 °C (blue) against the number of splits. The TMA exposure time ($t_{TMA} = 1.2$ s) was split x times while the water exposure time ($t_{Water} = 1.2$ s) was not split ($y = 0$). The purge times were 10 s for both precursors. The error bar denotes the standard deviation of Al_2O_3 thickness in a 6-in. wafer. (For interpretation of the references to colour in this figure legend, the reader is referred to the web version of this article.)

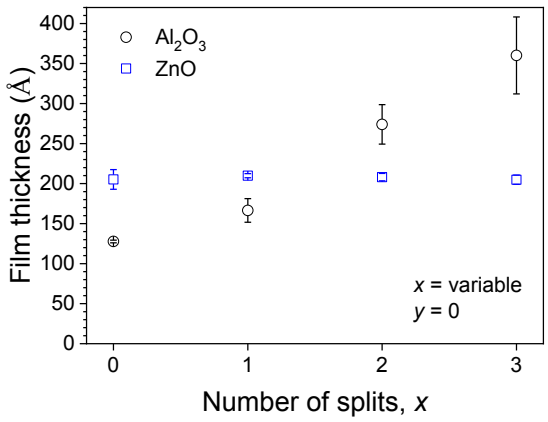

Fig. 3. Thickness variations of Al_2O_3 (circle) and ZnO (square) films grown for 100 cycles at 150 °C against the number of splits. For Al_2O_3 ALD, the TMA exposure time (t_{TMA} = 1.2 s) was split x times while the water exposure time (t_{Water} = 1.2 s) was not split (y = 0). For ZnO ALD, the DEZ exposure time (t_{DEZ} = 1.2 s) was split x times while the water exposure time (t_{Water} = 1.2 s) was not split (y = 0). All purge times were 10 s for both precursors. The error bar denotes the standard deviation of Al_2O_3 thickness in a 6-in. wafer.

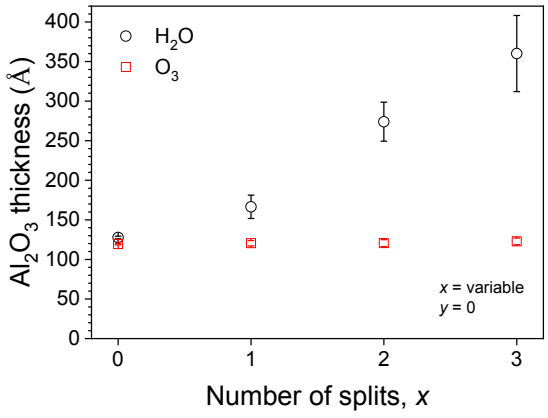

Fig. 4. Al_2O_3 thickness grown for 100 cycles at 150 °C using TMA/water (circle) and TMA/ozone (square) against the number of splits. The TMA exposure time (t_{TMA} = 1.2 s) was split x times while the exposure time of oxygen precursor (t_{Water} = 1.2 s or t_{Ozone} = 1.2 s) was not split (y = 0). All purge times were 10 s for both precursors. The error bar denotes the standard deviation of Al_2O_3 thickness in a 6-in. wafer.

GPC are TMA exposure and its Ar purge steps. To find evidence that the dimeric interaction and the residual water molecules cooperatively contribute to the unusually high GPC, mass spectra were obtained in the mass/charge (m/z) range of 15–145 at 80 °C using QMS during the TMA exposure and Ar purge steps (top panel in Fig. 5.). The bottom panel in Fig. 5 shows the magnified spectra in the m/z range of 60–140 for clarity, and the relative abundances of the principal fragments are listed in Table 1.

Mass spectrum in Fig. 5a was obtained at 1 s after the onset of TMA exposure onto the hydroxylated surface which was exposed to water for 40 s and then purged for 560 s. According to a previous report by Winters et al. [35], the most abundant peak from TMA was observed at m/z = 57 for the monomeric fragment of $Al(CH_3)_2^+$ and the dimeric species was detected in extremely low abundance for $Al_2(CH_3)_5^+$ species (m/z = 129) (see Table 1). However, the spectrum (Fig. 5a) obtained during the TMA exposure under the presence of a hydroxylated surface (and residual H_2O) shows some differences in the detected fragments and their relative abundances (Table 1). The strongest peak among Al-containing species in Fig. 5a was observed at m/z = ~57.5, which is

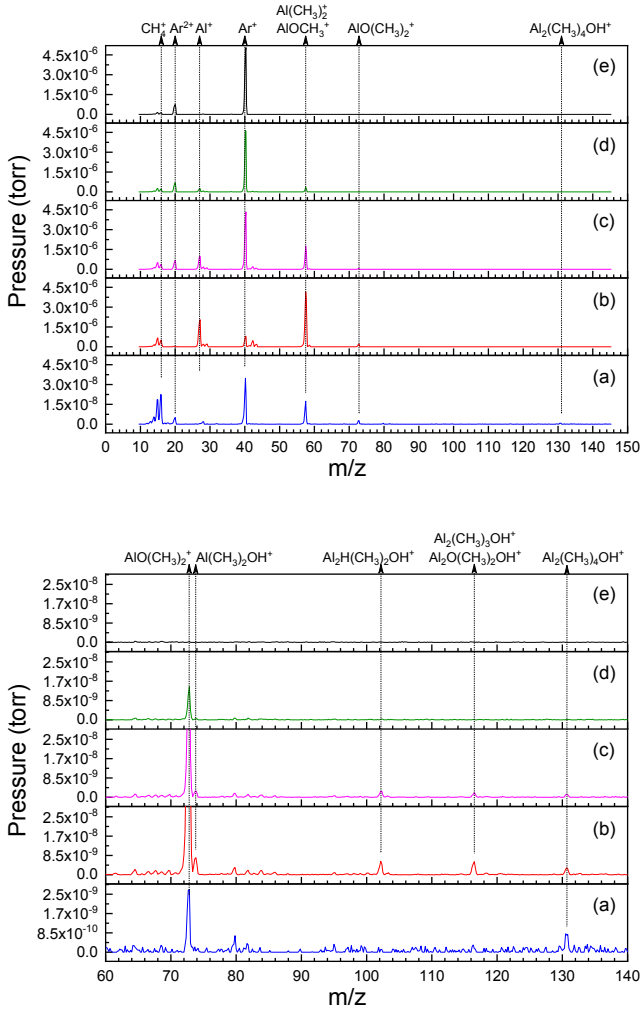

Fig. 5. Mass spectra (top panel) and their magnified spectra (bottom panel) during TMA exposure and Ar purge steps at 80 °C. (a) mass spectrum at 1 s after the onset of TMA exposure onto the hydroxylated surface. (b–e) Mass spectra at 1 s (b), 80 s (c), 200 s (d), and 360 s (e) after the onset of Ar purge after the TMA exposure for 40 s.

assigned to a mixture of $Al(CH_3)_2^+$ (m/z = 57) and $AlOCH_3^+$ (m/z = 58) species. The abundance of $Al(CH_3)_3^+$ (m/z = 72) was extremely low, but rather $AlO(CH_3)_2^+$ (m/z = 73) was detected with the second-highest abundance among Al-containing species. Furthermore, the dimeric fragment of TMA was detected at m/z = 131 rather than m/z = 129 of the $Al_2(CH_3)_5^+$ species. The peak at m/z = 131 is believed to be due to the presence of $Al_2(CH_3)_4OH^+$ species in which the OH group is bridged between two Al atoms in the dimer (see Table S1). The detection of H_2O with a non-negligible relative abundance supports the existence of residual water during the TMA exposure step.

During the TMA exposure step, the fragments of methane evolved by the ligand exchange reaction were observed at m/z = 15 and 16 with high relative abundances (see the top panel of Fig. 5a and Table 1). However, the methane fragments became relatively less abundant during the Ar purge step (see the top panel of Fig. 5b–e and Table 1). This indicates the ligand exchange reaction was almost completed before the Ar purge step. The dimeric fragments containing the OH group were additionally observed at m/z = 116.5 and m/z = 102 during the Ar purge. The former is assigned to a mixture of $Al_2O(CH_3)_2OH^+$ and $Al_2(CH_3)_3OH^+$ species, and the latter to $Al_2H(CH_3)_2OH^+$ species (see Table S1).[37–39] Their intensities decrease with the purge time (see the bottom panel of Fig. 5b–c). In addition, dimethylaluminum hydroxide (DMAH) was detected at m/z = 74 due to the presence of

Table 1
Relative abundances of the principal fragments formed from TMA in this work and Ref. [35].

Fragments[a]	*m/z*	Relative abundances		
		Fig. 5a	Fig. 5b	Ref. [35]
$Al_2(CH_3)_4OH^+$	131	4.3	<0.1	–
$Al_2(CH_3)_5^+$	129	–	–	0.2
$Al_2O(CH_3)_2OH^+$	117	–	0.1	–
$Al_2(CH_3)_3OH^+$	116			–
$Al_2H(CH_3)_2OH^+$	102	–	0.1	–
$Al(CH_3)_2OH^+$	74	–	0.2	–
$AlO(CH_3)_2^+$	73	15.9	5.3	–
$Al(CH_3)_3^+$	72	–	–	4.9
$AlOCH_3^+$	58	100	100	–
$Al(CH_3)_2^+$	57			100
$AlH(CH_3)^+$	43	–	4.7	3.4
$Al(CH_3)^+$	42	–	11.4	6.3
$Al(CH_2)^+$	41	–	–	1.0
AlH_2^+	29	–	5.3	2.3
AlH^+	28	10.8	4.8	–
Al^+	27	3.1	49.3	36.5
H_2O	18	5.9	< 0.1	–
CH_4^+	16	127.6	12.1	–
CH_3^+	15	106.3	16.3	21.3

[a] Structures of the listed fragments or alternative species for each value of *m/z* were listed in Table S1.

residual H_2O. Halls and co-workers proposed DMAH as a side-reaction product between TMA and residual H_2O which was responsible for the formation of the interfacial SiO_x layer in ALD of Al_2O_3 on Si [36]. From the observations of the OH– and O-containing species in dimeric and monomeric fragments, it is inferred that TMA (monomer and/or dimer) reacts incompletely with the residual H_2O in the gas phase or on the surface to form methylaluminoxane (MAO)-like clusters.

MAO is a generic term for the products of *incomplete hydrolysis* of TMA. MAOs play a critical role as an activator in catalytic olefin polymerization [40]. The formation of MAOs can be expressed as $0.5(n+m)Al_2(CH_3)_6 + nH_2O \rightarrow (CH_3AlO)_n(Al(CH_3)_3)_m + 2nCH_4$ where n = degree of oligomerization and m = number of associated TMA molecules [41,42]. If all TMA molecules are dissociated from MAO, its chemical formula is simplified to $(CH_3AlO)_n$, and the methylaluminumoxide (MAOx, CH_3AlO) is the structural unit of MAO. Despite decades of active research, the structures, compositions, formation mechanisms, and catalysis of MAOs are still controversial [40]. However, it is generally accepted that MAO clusters have oligomeric structures of various shapes as n and m increase in the formula of $(CH_3AlO)_n(Al(CH_3)_3)_m$. Interestingly, the repeating moiety (CH_3AlO) of MAO is also found in the chemical adsorption step (Eq. (1)) of TMA in Al_2O_3 ALD. The *incomplete hydrolysis* of TMA in Eq. (1) is controlled by the limited number of hydroxyl groups on the surface. However, the CH_3AlO moiety is completely hydroxylated to form Al_2O_3 layers upon exposure to water (Eq. (2)).

According to a recent report on the MAO formation by Glaser et al. [39], the incomplete hydrolysis of TMA initially results in the formation of DMAH ($Al(CH_3)_2OH$) as shown in Scheme 2. The structural unit MAOx (CH_3AlO) is formed from DMAH by its intramolecular 1,2-elimination of CH_4. Their dimeric aggregates with TMA or another DMAH play the role of intermediate in the initial steps of MAO formation.[39] All OH– and O-containing dimeric or monomeric fragments in Table 1 (or Table S1) can be found in Scheme 2 or be formed by fragmentation (see Scheme S1). This supports that the dimeric nature of TMA and TMAH cooperatively contributes to the incomplete hydrolysis of TMA by the residual H_2O for the formation of MAO-like clusters. In addition, methane gas is evolved in several steps of the MAO formation according to Scheme 2 (Ref. [39]). Therefore, the methane fragments detected during the prolonged Ar purge step (top panel of Fig. 5b–e) may be attributed to the formation of MAO-like clusters as well as the ligand exchange reaction.

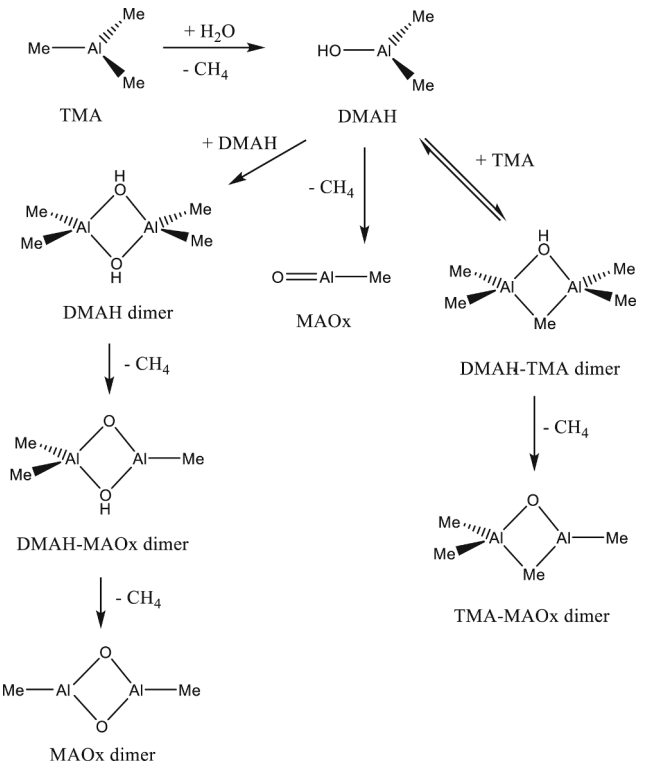

Scheme 2. Initial steps of MAO formation reported in Ref. [39] (Me = CH_3).

The mass spectrum of Fig. 5b, obtained at 1 s after the onset of Ar purge step, shows the relative abundance of the dimeric fragment ($Al_2(CH_3)_4OH^+$) is largely reduced to <0.1 comparting to the value (4.3) of Fig. 5a. Considering the relative abundance was referenced to the peak intensity of the monomeric fragments ($AlOCH_3^+$ and $Al(CH_3)_2^+$), this reduction indicates that the abundances of the dimeric fragments more rapidly decreases than the monomeric fragments during the purge step. The higher abundance of the monomeric fragments during the purge step is due to the dissociation of dimeric adsorbates as previously reported [29]. It is expected that the monomers of TMA and DMAH in the purging step may enable the formation of MAO-like clusters under the existence of residual H_2O. A plausible pathway for the formation of MAO-like clusters by split exposure of TMA in the presence of residual H_2O was shown as an example in Scheme S2. Even though the mechanism for the abnormally high GPC still remains elusive, it is inferred that the formation of DMAH and the dimeric interaction of the Al-containing species via the bridged methyl and/or hydroxyl groups contribute to the formation of MAO-like clusters on the surface and subsequently they are completely hydroxylated to form Al_2O_3 layers upon exposure to water.

4. Conclusion

The GPC of Al_2O_3 ALD using TMA and water was investigated by modifying the ALD sequence to split the TMA exposure time while keeping the water exposure time constant. Abnormally high GPC was observed at 80 and 150 °C, but not at 250 °C. When ozone was used instead of water, no abnormally high GPC was observed by splitting the TMA exposure time. In addition, there was no thickness increase by splitting the DEZ exposure time in ZnO ALD using DEZ with a monomeric structure. Therefore, the abnormally high GPC is believed to be due to the cooperative effect of the dimeric nature of TMA and the residual H_2O. This is supported by the observations of the OH– and O-containing dimeric aggregates during the TMA exposure and purge steps. As a plausible pathway, we suggest that the formation of MAO-like clusters may be involved in the abnormally high GPC.

CRediT authorship contribution statement

So-Yeon Ham: Writing – original draft, Conceptualization, Investigation. **Zhenyu Jin:** Validation. **Seokhee Shin:** Resources. **Minseo Kim:** Formal analysis. **Mingyu Seo:** Resources, Validation. **Yo-Sep Min:** Supervision, Writing – review & editing.

Declaration of Competing Interest

The authors declare that they have no known competing financial interests or personal relationships that could have appeared to influence the work reported in this paper.

Acknowledgments

This work was supported by Konkuk University in 2017.

Appendix A. Supplementary material

Supplementary data to this article can be found online at https://doi.org/10.1016/j.apsusc.2021.151282.

References

[1] S.M. George, Atomic layer deposition: an overview, Chem. Rev. 110 (1) (2010) 111–131.
[2] V. Crerners, R.L. Puurunen, J. Dendooven, Conformality in atomic layer deposition: current status overview of analysis and modeling, Appl. Phys. Rev. 6 (2019), 021302.
[3] H.-Y. Lee, C.J. An, S.J. Piao, D.Y. Ahn, M.-T. Kim, Y.-S. Min, Shrinking core model for Knudsen diffusion-limited atomic layer deposition on a nanoporous monolith with an ultrahigh aspect ratio, J. Phys. Chem. C 114 (43) (2010) 18601–18606.
[4] G. He, X. Chen, Z. Sun, Interface engineering and chemistry of Hf-based high-k dielectics on III-V substrates, Surf. Sci. Rep. 68 (2013) 68–107.
[5] G. He, J. Liu, H. Chen, Y. Liu, Z. Sun, X. Chen, M. Liu, L. Zhang, Interface control and modification of band alignment and electrical properties of HfTiO/GaAs gate stacks by nitrogen incorporation, J. Mater. Chem. C 2 (27) (2014) 5299–5308.
[6] Modulating the interface quality and electrical properties of HfTiO/InGaAs gate stack by atomic-layer-deposition-derived Al2O3 passivation layer, ACS Appl. Mater. Interfaces 6 (2014) 22013–22025.
[7] R.L. Puurunen, Growth per cycle in atomic layer deposition: real application examples of a theoretical model, Chem. Vap. Dep. 9 (6) (2003) 327–332.
[8] C.D. Travis, R.A. Adomaitis, Modeling ALD surface reaction and process dynamics using absolute reaction rate theory, Chem. Vap. Deposition 19 (1-3) (2013) 4–14.
[9] C.S. Hwang, Atomic Layer Deposition for Semiconductors, Springer, New York, NY, 2014.
[10] D. Hausmann, J. Becker, S. Wang, R.G. Gordon, Rapid vapor deposition of highly conformal silica nanolaminates, Science 298 (2002) 402–406.
[11] T. Muneshwar, K. Cadien, $A_xBA_xB\ldots$ pulsed atomic layer deposition: numerical growth model and experiments, J. Appl. Phys. 119 (2016), 085306.
[12] T. Muneshwar, K. Cadien, Surface reaction kinetics in atomic layer deposition: an analytical model and experiements, J. Appl. Phys. 124 (2018), 095302.
[13] H. Wang, Z. Wang, X. Xu, Y. Liu, C. Chen, P. Chen, W. Hu, Y. Duan, Multiple short pulse process for low-temperature atomic layer deposition and its transient steric hindrance, Appl. Phys. Lett. 114 (2019), 201902.
[14] A.C. Dillon, A.W. Ott, J.D. Way, S.M. George, Surface chemistry of Al_2O_3 deposition using $Al(CH_3)_3$ and H_2O in a binary reaction sequence, Surf. Sci. 322 (1-3) (1995) 230–242.
[15] A.W. Ott, J.W. Klaus, J.M. Johnson, S.M. George, Al_2O_3 thin film growth on Si(100) using binary reaction sequence chemistry, Thin Solid Films 292 (1997) 135–144.
[16] M.D. Groner, F.H. Fabreguette, J.W. Elam, S.M. George, Low-temperature Al_2O_3 atomic layer deposition, Chem. Mater. 16 (4) (2004) 639–645.
[17] L. Henn-Lecordier, M. Anderle, E. Robertson, G.W. Rubloff, Impact of parasitic reactions on wafer-scale uniformity in water-based and ozone-based atomic layer deposition, J. Vac. Sci. Technol. A 29 (5) (2011) 051509, https://doi.org/10.1116/1.3620421.
[18] H. Salami, A. Poissant, R.A. Adomaitis, Anomalously high alumina atomic layer deposition growth per cycle during trimethylaluminum under-dosing conditions, J. Vac. Sci. Technol. A 35 (1) (2017) 01B101, https://doi.org/10.1116/1.4963368.
[19] A.W. Laubengayer, W.F. Gilliam, The alkyls of the third group elements. I. vapor phase studies of the alkyls of aluminum, gallium and indium, J. Am. Chem. Soc. 63 (1941) 477–479.
[20] C.H. Henrickson, D.P. Eyman, Lewis acidity of alanes. interactions of trimethylalane with sulfides, Inorg. Chem. 6 (8) (1967) 1461–1465.
[21] G.S. McGrady, J.F.C. Turner, R.M. Ibberson, M. Prager, Structure of the trimethylaluminum dimer as determined by powder neutron diffraction at low temperature, Organometallics 19 (21) (2000) 4398–4401.
[22] T. Ogawa, Vibrational assignments and normal vibrations of trimethylaluminum, Spectrochim. Acta A 24 (1968) 15–20.
[23] D. Berthomieu, Y. Bacquet, L. Pedocchi, A. Goursot, Trimethylaluminum dimer structure and its monomer radical cation: a density functional study, J. Phys. Chem. A 102 (1998) 7821–7827.
[24] B.A. Hendriksen, D.R. Pearce, R. Rudham, Heats of adsorption of water on α- and γ-alumina, J. Catal. 24 (1972) 82–87.
[25] A.C. Engelsberg, J.J. Chera, G.M. Korenowski, Adsorbed TMA on dielectric oxide surfaces, Mat. Res. Soc. Symp. Proc. 101 (1987) 159–164.
[26] W.R. Salaneck, R. Bergman, J.-E. Sundgren, A. Rockett, T. Motooka, J.E. Greene, Adsorption of tri-methyl aluminum molecules on silicon, Surf. Sci. 198 (3) (1988) 461–472.
[27] F. Lee, T.R. Gow, R. Lin, A.L. Backman, D. Lubben, R.I. Masel, The decomposition of trimethylgallium and trimethylaluminum on Si(100), Mat. Res. Soc. Symp. Proc. 131 (1989) 339–344.
[28] T.R. Gow, R. Lin, L.A. Cadwell, F. Lee, A.L. Backman, R.I. Masel, Decomposition of trimethylaluminum on Si(100), Chem. Mater. 1 (1989) 406–411.
[29] C. Soto, R. Wu, D.W. Bennett, W.T. Tysoe, Infrared spectroscopy of trimethylaluminum and dimethylaluminum chloride adsorbed on alumina, Chem. Mater. 6 (10) (1994) 1705–1711.
[30] S.S. Masango, R.A. Hackler, A.-I. Henry, M.O. McAnally, G.C. Schatz, P.C. Stair, R. P. Van Duyne, Probing the chemistry of alumina atomic layer deposition using operando surface-enhanced Raman spectroscopy, J. Phys. Chem. C 120 (7) (2016) 3822–3833.
[31] R.A. Hackler, M.O. McAnally, G.C. Schatz, P.C. Stair, R.P. Van Duyne, Identification of dimeric methylalumina surface species during atomic layer deposition using operando surface-enhanced Raman spectroscopy, J. Am. Chem. Soc. 139 (6) (2017) 2456–2463.
[32] J. Bacsa, F. Hanke, S. Hindley, R. Odedra, G.R. Darling, A.C. Jones, A. Steiner, The solid-state structures of dimethylzinc and diethylzinc, Angew. Chem. Int. Ed. 50 (49) (2011) 11685–11687.
[33] D.N. Goldstein, J.A. McCormick, S.M. George, Al_2O_3 atomic layer deposition with trimethylaluminum and ozone studied by in situ transmission FTIR spectroscopy and quadrupole mass spectrometry, J. Phys. Chem. C 112 (49) (2008) 19530–19539.
[34] J. Kwon, M. Dai, M.D. Halls, Y.J. Chabal, Detection of a formate surface intermediate in the atomic layer deposition of high-k dielectrics using ozone, Chem. Mater. 20 (2008) 3248–3250.
[35] R.E. Winters, R.W. Kiser, Ionization and fragmentation of dimethylzinc, trimethylaluminum, and trimethylantimony, J. Organometal. Chem. 10 (1) (1967) 7–14.
[36] M.D. Halls, K. Raghavachari, M.M. Frank, Y.J. Chabal, Atomic layer deposition of Al2O3 on H-passivated Si: $Al(CH_3)_2OH$ surface reactions with H/Si(100)-2×1, Phys. Rev. B 68 (2003), 161302.
[37] J. Tanaka, S.R. Smith, Mass spectra of bridge-bonded aluminum compounds, Inorg. Chem. 8 (2) (1969) 265–270.
[38] Y.S. Hiraoka, M. Mashita, Ab initio study on the dimer structures of trimethylaluminum and dimethylaluminumhydride, J. Cryst. Growth 145 (1-4) (1994) 473–477.
[39] R. Glaser, X. Sun, Thermochemistry of the initial steps of methylaluminoxane formation. aluminoxanes and cycloaluminoxanes by methane elimination from dimethylaluminoxane hydroxides and its dimeric aggregates, J. Am. Chem. Soc. 133 (2011) 13323–13336.
[40] E.Y.X. Chen, T.J. Marks, Cocatalysts for metal-catalyzed olefin polymerization: activators, activation processes, and structure-activity relationships, Chem. Rev. 100 (2000) 1391–1434.
[41] M. Linnolahti, A. Laine, T.A. Pakkanen, Screening the thermodynamics of trimethylaluminum-hydrolysis products and their co-catalytic performance in olefin-polymerization catalysis, Chem. Eur. J. 19 (22) (2013) 7133–7142.
[42] M. Linnolahti, S. Collins, Formation, structure, and composition of methylaluminoxane, ChemPhysChem 18 (23) (2017) 3369–3374.

Supporting Information

Investigation of abnormally high growth-per-cycle in atomic layer deposition of Al_2O_3 from trimethylaluminum and water

So-Yeon Ham,† Zhenyu Jin, Seokhee Shin, Minseo Kim, Mingyu Seo and Yo-Sep Min*

Department of Chemical Engineering, Konkuk University, 120, Neungdong-Ro, Gwangjin-Gu, Seoul 05029, Korea

*Yo-Sep Min. E-mail: ysmin@konkuk.ac.kr

†Current affiliation: So-Yeon Ham, Materials Science and Engineering Program, University of California San Diego, 9500 Gilman Drive, La Jolla, San Diego, CA 92093, USA

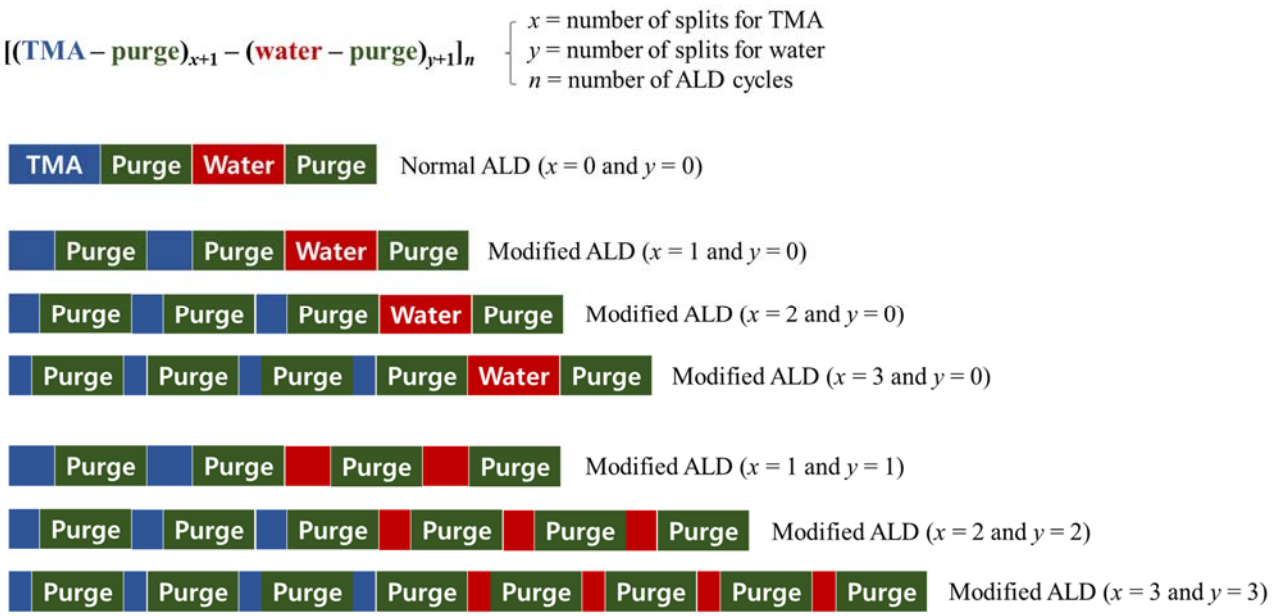

Figure S1. Representative ALD sequences of the normal and the modified processes performed in this work.

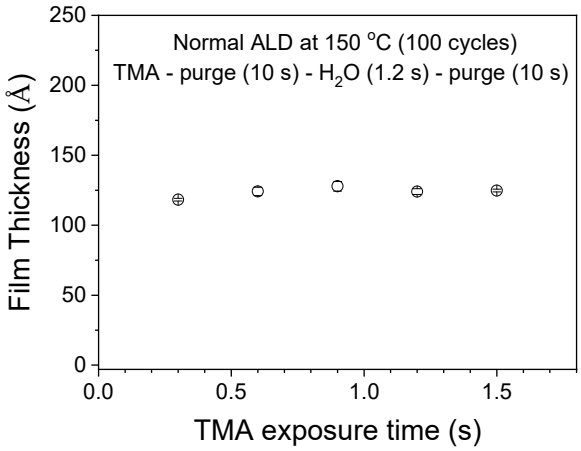

Figure S2. Al_2O_3 thickness variation as a function of TMA exposure time. Al_2O_3 films were grown at 150 °C for 100 cycles by the normal process ($x = y = 0$).

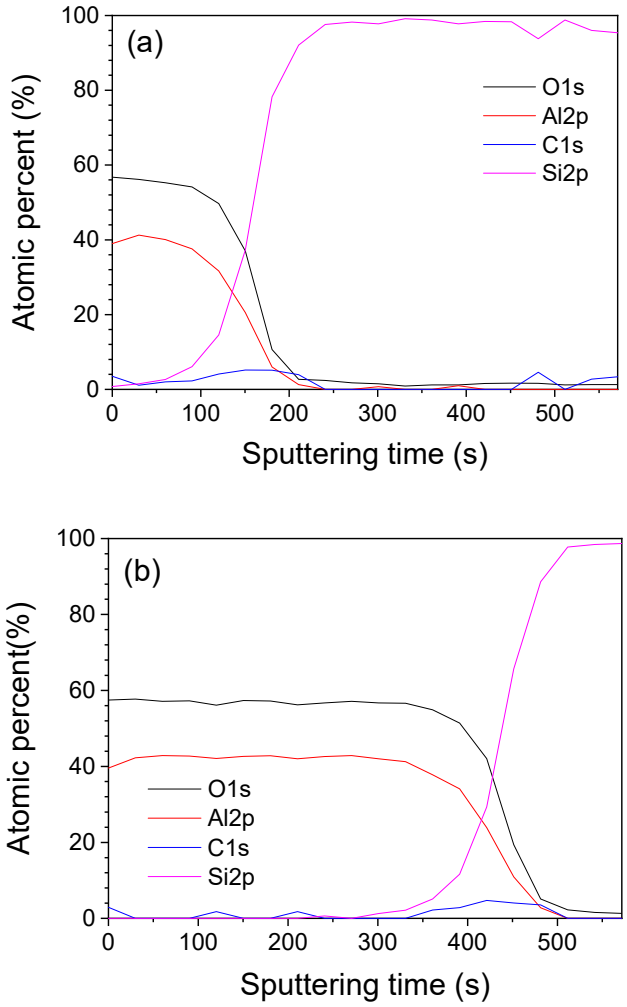

Figure S3. XPS depth profiles of Al_2O_3 thin films grown for 100 cycles at 80 °C by (a) the normal process (x = y = 0) and (b) modified process (x = 3 and y = 0).

Table S1. Structures of the fragments and alternative species for each value of m/z listed in Table 1.

m/z	Fragments	Alternative species
(a) m/z = 131	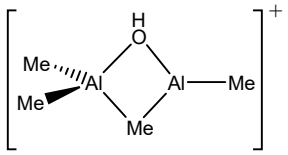	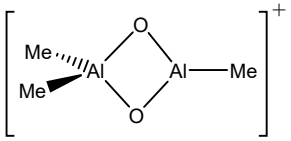
(b) m/z = 129	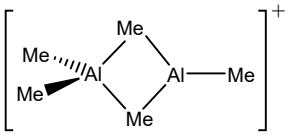	
(c) m/z = 117	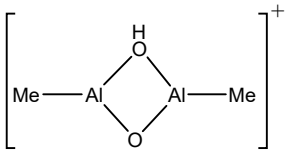	
(d) m/z = 116	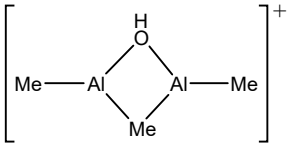	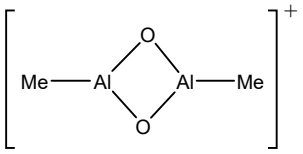
(e) m/z = 102	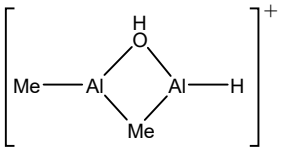	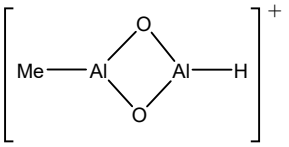
(f) m/z = 74	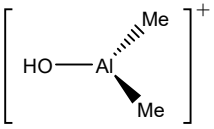	
(g) m/z = 73	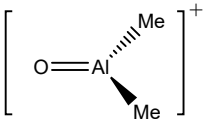	
(h) m/z = 72	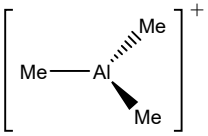	
(i) m/z =58	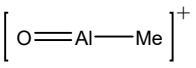	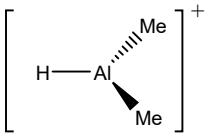
(j) m/z = 57	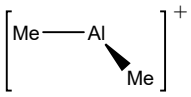	

Scheme S1. The plausible fragmentation process for each fragment listed in Table S1.

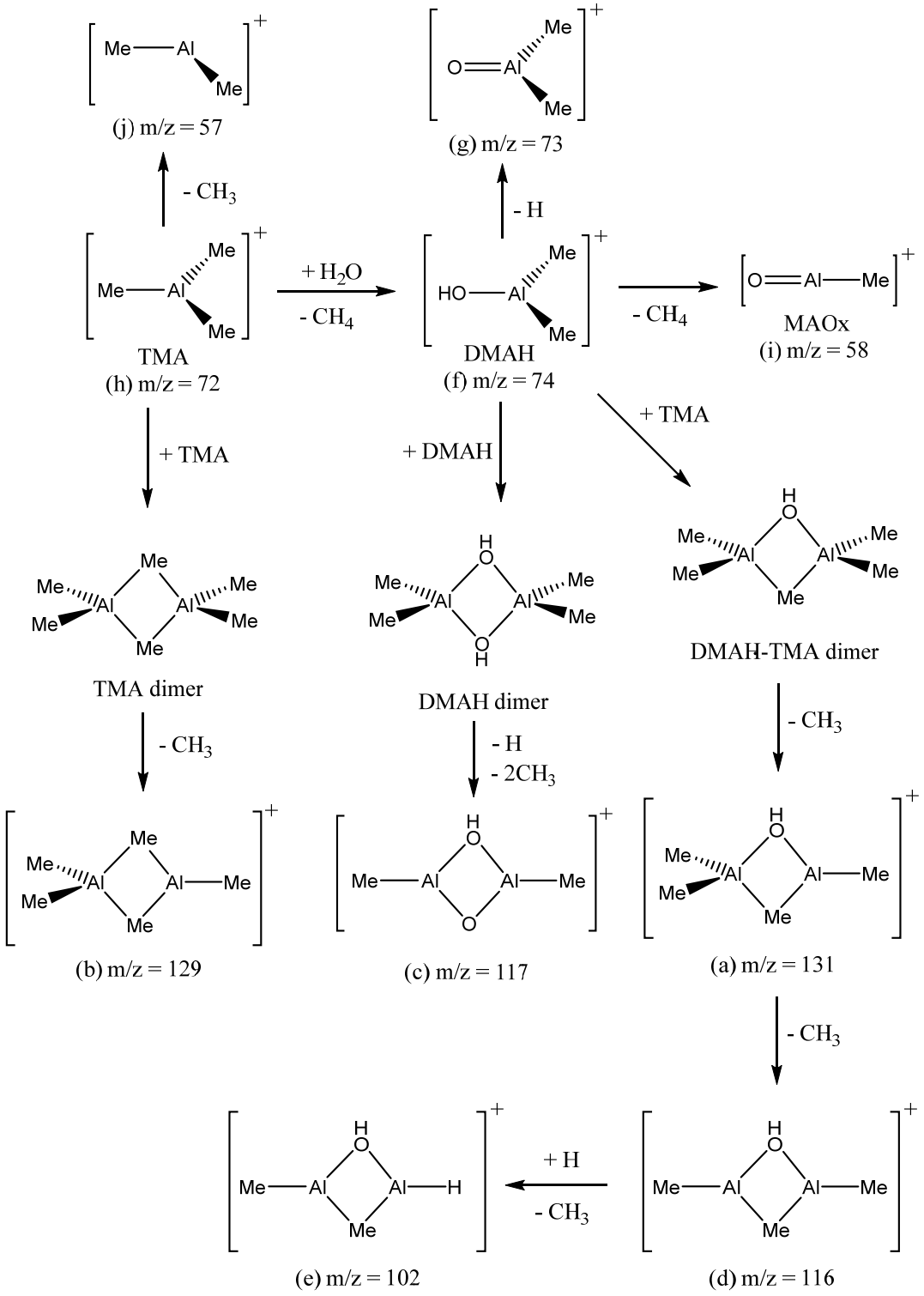

Scheme S2. A Plausible pathway for the formation of MAO-like clusters by split exposure of TMA in the presence of residual H_2O.